NASA TECHNICAL MEMORANDUM

NASA TM X-52886

NASA TM X-52886

USE OF THE COMPUTER IN DESIGN OF GAS TURBINE MAINSHAFT SEALS FOR OPERATION TO 500 FT/SEC (122 M/SEC)

by L. P. Ludwig, J. Zuk, and R. L. Johnson
Lewis Research Center
Cleveland, Ohio

TECHNICAL PAPER proposed for presentation at
Twenty-sixth Annual Meeting of the National Conference on Fluid Power
and the Tenth Annual Meeting of the Fluid Power Society
Chicago, Illinois, October 13-15, 1970

USE OF THE COMPUTER IN DESIGN OF GAS TURBINE MAINSHAFT SEALS FOR OPERATION TO 500 FT/SEC (122 M/SEC)

by L. P. Ludwig, J. Zuk, and R. L. Johnson

National Aeronautics and Space Administration
Lewis Research Center
Cleveland, Ohio

E-5917

ABSTRACT

Computer programmed analyses of the seal temperature field, elastic displacements and seal force balance were used in an iterative design procedure to arrive at a final mainshaft seal design. For high speeds, temperatures and pressures in advanced engines, the sealing surfaces must not operate with rubbing contact. Hence, self-acting lift pads were incorporated to achieve positive separation of the sealing surfaces. Therefore, a small gas film separating the sealing surfaces is achieved and the associated high gas-film-stiffness forces the seal nosepiece to dynamically track the runout motion of the seal face. Analysis revealed that the pressure profile across the sealing dam was significantly affected by sealing face deformation and that choked flows occurs at pressure ratio of greater than 4 to 1. The effect of this face deformation and choked flow was considered in establishing the seal force balance. Further, to mitigate the effects of thermal deformation it was necessary to structurally isolate the seat from the shaft. The role of the computer in the seal design is discussed. Tests confirm operation as predicted by the design analysis.

SUMMARY

A shaft face seal with self-acting geometry was designed utilizing computer analysis. These seals are for sumps in aircraft gas turbine engines. The self-acting geometry provides lift forces to separate (no rubbing contact) the sealing surfaces at the operating speed. Noncontact

operation is deemed necessary for high speeds, pressures and temperatures. Since the amount of lift is on the order of 0.0005 inch (0.00127 cm), the leakage is acceptable. To operate without rubbing contact, the seal force balance had to be controlled within the load limits of the self-acting geometry. Therefore, a necessary design goal was to minimize sealing face thermal and mechanical deformation. (Face deformations can markedly alter seal force balance.) These deformations were found by computer analyses. These analyses led to mitigation of thermal deformations by thermal shielding and by use of molybdenum alloy which has thermal deformations about 1/7 that of conventional seal materials. In addition the seat was structurally isolated from the shaft to reduce the deformation effects of the shaft thermal growth. Also, by clamping the seat through a bellows with a predetermined axial force, deformation due to assembly clamping was minimized.

Load carrying capacity of the self-acting geometry was investigated (computer programmed) for various recess depths, film thicknesses, angular deformations and number of self-acting pad geometries. It was found that the self-acting pad geometries had characteristically steep gradient of lift force versus film thickness. This steep gradient is advantageous in that if the seal tends to open, the lift force drops off rapidly, hence, the closing force increases rapidly; and if the seal tends to close, the opposite effect occurs. Therefore, a small operating film thickness is maintained.

The seal leakage rates and pressure profiles across the seal dam (found by computer programs) were determined for typical operating conditions and for various design parameters (such as dam width, face angular deformation, film thickness, and choked flow). It was found that the pressure profile was significantly affected by face deformation and that choked flow occurs at pressure ratios of 4 to 1 and greater.

Tests confirm operation as predicted by the design analysis.

INTRODUCTION

Aircraft gas turbine engines have shaft seals which restrict gas leakage into the bearing sumps. Various types of shaft seals are used; some engines employ labyrinth seals exclusively, others use face and/or circumferential type contact seals. Labyrinth seals have disadvantages of high leakage rates and associated debris entrainment; long operating life and reliability are the chief advantages as compared to face and circumferential type seals which are limited in pressure and speed capability because of rubbing contact. For conventional face contact seals, current limits are near 125 psi (86.1 N/cm^2), 350 ft/sec (107 m/sec) and 800° F (700 K) (ref. 1); pressure and speed capabilities of circumferential seals are near that of face seals.

Recent developments in seals with self-acting lift augmentation (ref. 2) promises a seal with the speed capability of labyrinth seals and the low leakage capability of contact seals. This self-acting lift seal is similar in construction to that of a conventional face seal except that the self-acting geometry acts to keep the sealing surfaces separated, thus, the seal has high speed potential. Rubbing occurs only on start-up and shut-down. The lift force of the self-acting geometry also provides positive gas film stiffness (ref. 3) which allows the nosepiece to dynamically track the runout motions of the seat face. Further, because of high gas film stiffness the self-acting geometry inherently operates with a small face separation, thus, the mass leakage flow through the seal is much less than that of a labyrinth seal.

A vital design consideration in the self-acting face seal (or conventional seal) is the relative displacement of the seal parts due to mechanical forces and thermal growth. As pointed out by reference 3, small relative displacement of seal parts can have a significant affect on the nosepiece force balance. A primary objective of the seal design effort, therefore, is to minimize the relative displacements of the seal parts.

In particular, deformation due to thermal gradients are a major problem. Therefore, in the seal design process, the thermal distribu-

tion of the seal assembly was repeatedly checked and design changes made until an acceptable distribution was obtained.

Also vital to performance is the gas film thickness which is a result of the mechanical and pneumatic forces acting on the seal and the lift force produced by the self-acting geometry (ref. 3). Therefore, a detailed analysis of seal forces was necessary in order to achieve a film thickness large enough to accommodate some thermal deformation and small enough to provide an acceptable leakage rate. Further, the gas film had to be small enough to provide the stiffness necessary to accommodate inertia forces due to the inherent runout of the face.

For the purpose of analysis, four design points were selected as representative of operating conditions in the advanced gas turbine (see table I). Consideration was given to a full scale type mainshaft seal of 7.05 inch (17.91 cm) mean sealing diameter. Extensive use was made of computer programs to determine the effect of various parameters on temperature distribution, displacement fields, stress fields, seal force balance and leakage.

DESCRIPTION OF FACE SEAL WITH SELF-ACTING GEOMETRY FOR LIFT AUGMENTATION

Figure 1 is a cross section of the final design configuration of the face seal with self-acting lift geometry. As with a conventional face seal it consists of a rotating seat (all rotating parts are marked with "w") which is attached to the shaft and a nonrotating nosepiece assembly that is free to move in an axial direction thus accommodating engine thermal expansion (axial). The piston ring type secondary seal is subjected only to the axial motion (no rotation) of the nosepiece assembly and several springs provide force to maintain contact at start and stop. In operation, the sealing faces are separated a slight amount (in the range of 0.0005 inch (0.00127 cm)) by action of the self-acting lift geometry, and gas leakage is from the high pressure side (i.d. of carbon nosepiece) across the sealing dam into the bearing sump. This gas leakage pressurizes the sump and assures proper scavenging of the

bearing lubricant. It should be noted that although the sealed gas temperature is high, tests have shown that considerable gas temperature drop occurs in the leakage flow so that the leakage into the sump does not pose a fire hazard when the seal is operating properly. Operation to 40 SCFM (1.05 std m^3/min) and 1200° F (922 K) sealed air temperature has been obtained without a sump fire.

As shown in figure 1, the seat is thermally and partially structurally isolated from the shaft by the following means:

(1) The radial spacer between the seat and shaft serves as a spring that mitigates the effect of nonuniform shaft thermal growth (radial) due to the axial thermal gradient. The effect of thermal movement is further attenuated by piloting the seat over its centroid.

(2) The bellows clamping spacer applies a predetermined clamping force (approximately 2000 lbf (8896 N), which is probably an order of magnitude less than clamping forces produced by the usual bearing lock nut assembly technique. Therefore, the deformation during assembly is minimized. The seat thermal design is tailored to minimize the axial thermal gradient. Use of a molybdenum alloy, instead of the conventional SAE 8740 or heat resistant alloy, provides a relatively low deformation criterion which is defined as the ratio of thermal expansion to thermal conductivity (ref. 4). The cooling oil flow path (see fig. 1) is also tailored to minimize the axial thermal gradient. By passing the cooling oil under the radial spacer, the first contact of the cooling oil with the seat is near the hotter face (face mated with nosepiece) of the seat. Analysis has shown that this oil route minimizes the thermal gradient. Centrifugal pumping action due to rotation and the 45 radial exit holes near the hot face assures even distribution of the cooling oil.

ROLE OF COMPUTER IN SEAL DESIGN

The seal assembly has a moderately complex geometry. The seal performs under severe conditions and multioperational points. Simple mathematical models are necessary for preliminary analysis but are

ultimately insufficient. Large-scale seal assembly testing, alone, for a parametric design study is prohibitive in both time and cost. However, programmed analyses utilizing computers can play an important role in the design of mainshaft seals with self-acting lift pad geometry.

Candidate seal designs can be screened by computer analysis. Computer analyses of seal temperature field, elastic displacements, self-acting geometry, seal force balance, and seal leakage rate information can be used in an iterative design procedure to arrive at a final seal design. (Some supporting small scale testing may compliment the analysis.) The computer design analysis can then be used with experience and intuition to arrive at a configuration to be tested which, hopefully, will meet the desired design objectives. Further testing may indicate additional modifications to improve performance. The computer can be useful in guiding design changes and interpretation of experimental results (especially at conditions very difficult or impossible to instrument).

The computer programs used in the seal analysis range from very simple calculations to more complicated solutions of large systems of differential equations. The programs utilize many numerical analysis techniques such as interpolation, numerical integration, and iterative solutions of nonlinear algebraic equations. The governing equation of the self-acting lift pad and thermal analysis were solved by the method of finite differences. The thermal and centrifugal stresses were found by the finite element method. Thus, a parametric design study may be made where many parameters are varied. This parametric analysis would be highly impractical by hand calculations. An example of the computer printout is shown in figure 2 from reference 8. The sealed pressure differential across the sealing dam is 50 psi for a diverging radial tilt of one milliradian. Note that the program prints out calculated variable values (found from the equations shown in table II), parameters such as Reynolds numbers and Knudsen numbers, and other useful information. Also note the printout stating that the formulation is not

valid for a range of specified input film thicknesses. These calculations were all performed in less than 0.1 minute.

Computer plotting of results is helpful and time saving. At the Lewis Research Center specified results can be plotted on microfilm. An example of this plot is shown in figure 3 where the Mach number values are shown plotted as a function of radial position along the sealing dam for several film thicknesses. A Calcomp computer plotter is also available. This plotter is especially useful for three dimensional graphs which are difficult to plot or visualize. An example of this type of plot is shown in figure 4. Here the self-acting lift pad geometry pressure distribution is shown. Note the effect of side leakage on the pressure distribution which is minimized by the shrouds.

The computer program references used in this design analysis include all details necessary to minimize the effort required for use on other computers. The computer programs are written in FORTRAN IV for the computer at Lewis Research Center, which is an IBM 7094II/7044 or 7040 direct computer. The programs are described in detail including all input and program variables and output options. Program flow charts are presented in detail and sample problems with computer printouts are given. Where possible program accuracy is compared with known exact solutions. The use of the computer in design of gas turbine mainshaft seals for operation at high speeds, temperatures and pressures will follow.

RESULTS AND DISCUSSION

Figure 5 is a typical calculated thermal map of the final seat configuration for the design operating conditions of 165 psia (114 N/cm^2 abs), 500 ft/sec (153 m/sec) and 800° F (700 K) sealed gas temperature. (design point 4). This thermal distribution was obtained by means of the computer program given in reference 5. Inspection of the temperature field reveals that the heat shields are effective in reducing the thermal gradient in the seat. As an example, the heat shield which protects the

seat face from the oil passing through the bearing has a calculated temperature of 427° to 492° F (493 to 529 K) and the adjacent seat face is 651° to 658° F (617 to 621 K). Thus, without this shield the seat face would be subjected to oil cooling and the seat gradient and corresponding deformation would be greater.

Figure 6 gives the calculated seat assembly stresses due to combined centrifugal and thermal effects. In general, about one half of the stress magnitude can be attributed to thermal effects, the rest arises from centrifugal effects. Thus, the thermal gradient, in addition to being a major factor in seat deformation, is also a significant factor in stress levels. Minimization of the seat thermal gradient is, therefore, the crux of the seat design problem. Figure 7 shows the calculated seat assembly displacement due to combined centrifugal and thermal effects, as is the case of the stresses, the thermal effects are significant. The important point is that the seat face which mates to the carbon nosepiece remains relatively square to the shaft centerline. The net calculated mating face deformation in the axial (z) direction is 0.0006 inch (0.00152 cm).

The nosepiece assembly (see figs. 1 and 8) consists of the carbon-graphite ring which is shrink fitted into a molybdenum retainer ring and this assembly in turn is piloted (located) by resilient ring attached to the carier (also molybdenum alloy). Molybdenum alloy is used in the carrier and retainer ring in order to minimize thermal deformation. (The relatively high density of molybdenum is a disadvantage in that the inertia forces associated with nosepiece movement are, therefore, higher). The carbon-graphite ring contains the self-acting geometry that consists of a series of shallow recesses arranged circumferentially around the seal under the sealing dam (fig. 8). It should be noted that the lift geometries are bounded at the inside and outside diameters by the sealed pressure P_1. This is accomplished by feed slots that connect the annular groove directly under the sealing dam with the sealed pressure (P_1).

The effect of the self-acting geometry on face seal operation is illustrated in figure 9, which depicts parallel sealing faces operating without rubbing contact because of a balance between the closing forces and the opening forces. If the seal tends to close, the self-acting force increases to prevent rubbing contact; thus, a condition of no rubbing contact can prevail except at startup and shutdown.

Self-Acting Lift Geometry Investigation

A single self-acting pad (shrouded step-type), which served as the mathematical model, is shown in figure 10(a). The radial width b of all pad geometries investigated was 0.20 inch (0.507 cm), and the length c was determined by the number of pads that could be arranged circumferentially under the sealing dam. Because of the large radius-to-pad with ratio r/b, the curvature was neglected in the mathematical model. Thus, the pad boundaries conform to a Cartesian coordinate system. The feed-groove width f was held constant for all pads. In the investigation the recess length-to-land length ratio R/L was varied between 0.4 and 1.8. Also, the effect (on load capacity) of recess depth (Δ) to film thickness (h) ratio was determined over the range of $(\Delta + h_m)/h_m = 1.52$ to 6.0. (All symbols are defined in appendix A.) Calculations of load capacity were made for the parallel film face and for the case with a 2-milliradian angular deformation. This angular deformation was chosen as a practical case that might occur as the result of thermal gradients. Figure 10(b) shows the actual dimensions of the final pad design.

The computer program listing in reference 6, which is valid for a shrouded lift pad, was used for this study. This computer program has been modified (as given in ref. 7) so that it can be used on the Lewis Research Center computer, and the input has been modified for NAMELIST to facilitate parametric design studies. The program solves the complete two-dimensional compressible flow Reynolds lubrication equation written in the P^2 form

$$\frac{\partial}{\partial X}\left(\frac{H^3}{2}\frac{\partial P^2}{\partial X}\right)+\frac{\partial}{\partial Y}\left(\frac{H^3}{2}\frac{\partial P^2}{\partial Y}\right)=\Lambda_x\frac{\partial(PH)}{\partial X}+\Lambda_y\frac{\partial(PH)}{\partial Y}$$

where

$$\Lambda_x=\frac{6\mu Ub}{P_a h_m^2} \qquad \Lambda_y=\frac{6\mu Vb}{P_a h_m^2}$$

A discussion of the use of the program for a nonparallel film is given in appendix A of reference 6.

The computer program was used to investigate the performance of various self-acting designs and to determine the effects of various parameter changes. Some of the parameters investigated were: (a) number of self-acting pads, (b) ratio of recess length to load length, (c) ratio of recess depth to film thickness, (d) effect of face angular deformation and (e) effect of recess depth on film stiffness. Figure 11 is an example of the data generated by the computer program. Here load capacity of the self-acting geometry is plotted as a function of film thickness for three of the design points listed in table I.

The calculations are for 20 pads and a recess depth of 0.001 inch (0.003 cm). The curves reveal a high film stiffness that is advantageous for seal operations; that is, at low film thicknesses, a high lift force is produced to prevent rubbing contact and at high film thicknesses, which would have high leakage, only a low lift force is produced. Thus, if the seal opens, the pad lift force drops off sharply, and the closing force acts to return the nose to the equilibrium position.

Sealing Dam Model

The sealing dam analysis is based on a sealing dam model described in detail in references 8 and 9. The model consists of two parallel, co-axial, circular rings in relative rotation at a constant speed

separated by a very narrow gap (fig. 12). A pressure differential exists between the ring's inner and outer radii. The cavities on either side (i.d. and o.d.) of the sealing dam are assumed to be constant pressure reservoirs.

See references 8 and 9 for details of the assumptions; however, the following pertinent comments should be noted:

1. The effect of the rotational flow on the hydrostatic radial flow is neglected. Equation (39) from reference 10 shows that this assumption is justified. For practical film thicknesses the calculated increase in leakage due to rotation would only be 2.6 percent for design point 1, 7.9 percent for design point 2 and 4.3 percent for design point 3.

2. For subsonic flow, Mach number $\leq 1/\sqrt{\gamma}$, the analysis of reference 8 will be used. This analysis finds an exact solution for this case when the viscous friction is balanced by the pressure drop. For this condition the entrance pressure drop is small, hence $P_1 = P_1'$ and $P_2 = P_2'$ (see fig. 12). The flow is basically isothermal for the film thickness range studied and the analysis yields the classical cubic dependence of mass flow on film thickness. Also this computer analysis enables small tilts of the sealing dam surfaces to be studied. These small tilts simulate seal face deformation which can be due to thermal, centrifugal, etc., effects. The equation used from this analysis are summarized in table II.

3. For flow approaching Mach 1 where the flow chokes, the inertia force neglected in reference 8 becomes important. Also the flow behaves more as an adiabatic flow rather than isothermal. The mathematics is very complex because of the nonlinearity of the inertia terms; thus an approximate quasi-one dimensional analytical model was constructed. In this model the viscous effects are represented by a mean friction factor which has been observed to be almost invariant under many an ensemble of fluid mechanics experiments, geometries, and conditions. See reference 9 for details. This mean friction factor is 24/Re and it can be derived from the exact analysis of reference 8 for subsonic flow.

The quasi-one dimensional flow model is valid for choked flow. (In practical seals the flow can be choked at the exit for pressure ratios greater than about 4:1.) It should be noted that the area expansion is negligible in this design since $A_{id}/A_{od} = 0.985$. Also there is a pressure drop at the entrance ($P_1' \neq P_1$) and when choking occurs at the exit then $P_2' \neq P_2$.

The results that are found were obtained by using the computer programs found in references 8 and 9. These two references appeared to be the best available models simulating the actual gas film seal.

Leakage Flow Rates

Figure 13 shows the relation between film thickness and gas leakage flow from the high pressure side into the sump (low pressure side). The calculations for these design points (table I) were obtained from the seal analysis computer programs (ref. 8 and 9), and are for a parallel surface sealing dam of 0.050-inch (0.127 cm) in radial width. For small film thickness 0.0002-inch (0.0005 cm) the leakage is small, in the range of 0.43 SCFM (2.06×10^{-4} SCMS) for design point 1. But because of the cubic dependence of leakage on film thickness, a slight change in film thickness significantly affects leakage. For design point 1 choking occurs for a film thickness of 0.00055-inch (0.00131 cm); the pressure ratio is approximately 4 to 1. Note that for larger gaps the leakage has a lesser than cubic dependence on gap height. A limiting case is a linear dependence which would be achieved when the film thickness is on the order of the sealing dam radial width of 0.050 inch (0.127 cm).

The computer program was also used to investigate the effect of changing the dam radial width. Also the program output provides a plot of the pressure profile (pressure change) across the dam, and as an example, figure 14 shows the pressure profile for parallel and for nonparallel sealing surfaces (and nonchoking condition). These pressure profiles are plotted (fig. 14) for mean film thicknesses of 0.0002-inch

(0.0005 cm) and 0.0004-inch (0.0010 cm) and for sealing face deformation of ±0.001 radians with the negative (-) deformation indicating a converging film in the leakage direction and a positive (+) deformation indicating a diverging film. The important point (see fig. 14) is that for the convergent film case, a decrease in film thickness results in greater area (larger opening force) under the pressure profile curve; thus, the convergent film has a positive film stiffness. Conversely, as shown by the figure 14 a divergent film has a negative film stiffness. This means that for a divergent film a film thickness decrease (which always occurs dynamically) will cause a decrease in opening force and, this decrease must be counterbalanced by a corresponding increase in lift force of the self-acting pads if a condition of no rubbing contact is to be maintained.

Figure 15 shows the pressure profiles along the sealing dam radial width found using the computer program in references 8 and 9 for parallel surfaces. For film thicknesses equal to or less than 0.0002 inch (0.0005 cm) the profile doesn't depend on film thickness; the flow is subsonic and the profiles are found from the isothermal viscous flow analysis of reference 8. When the flow is choked and the mean film thickness increases, the entrance pressure loss becomes significant; also the exit pressure is larger (choked flow) than the sump pressure and increases with film thickness. The pressure expands in an oscillatory manner to the sump pressure in the outer cavity.

Sealing Dam Opening Force

The area under the pressure profile curves (figs. 14 and 15) represents a force which tends to open the seal. This opening force is found by an integration of the pressure distribution across the sealing dam radial width. The integrations of the pressure distributions shown in figure 14 (design point 1) are plotted in figure 16. (The opening force is shown for convergent, parallel, and divergent surfaces.)

The change in seal opening force due to a divergent deformation is of particular interest because the divergent deformation is a natural

tendency (due to thermal gradient) in a gas turbine engine (ref. 3). Any decrease in seal opening force due to a divergent deformation must be compensated by the lift pads; the magnitude of opening force changes, therefore, help determine the lift pad requirements. Of interest is the effect of seal dam width on seal opening force and table III shows the opening force for an average film thickness change of 0.0002-inch (0.0005 cm) for a divergent deformation of +0.002 radians. Three dam widths (see table III) typical of conventional face seals were chosen for comparative purposes. As shown the smallest dam width (0.050-inch (0.127 cm)) has the smallest opening force change when the film thickness changes. Thus, smaller dam widths are desirable because smaller force changes are produced under dynamic conditions when the film thickness is changing.

GROSS SEAL CHARACTERISTICS

The gas film seal operating film thicknesses can be found by equating the closing forces with the opening forces. The closing forces are comprised of the spring (mechanical) force and a hydrostatic (pneumatic) closing force. (A spring force of 6.6 pounds was chosen.) The hydrostatic closing force is determined by the bore diameter against which the secondary seal (piston ring) mates (fig. 1). This diameter changes with temperature and should be considered in the force balance calculations.

The results are summarized on table IV. Note that a leakage of 25 SCFM (1.18×10^{-3} SCMS) or less can be expected for the three design points shown. This is about an order of magnitude less than that achieved by conventional labyrinth seal practice.

TEST RESULTS

Recent NASA sponsored tests of the shaft face seal with self-acting lift augmentation have demonstrated the feasibility of operation at gas

temperatures up to 1200° F, pressure differentials across the seal up to 250 psi, and relative surface speeds up to 450 ft/sec. These tests simulated the engine operating conditions as represented by four design points in table I. The seal appears to be operating as predicted by the design analysis. Figure 17 shows the nosepiece seal assembly after the 120 hour endurance test. Figure 18 shows a closeup of the carbon nosepiece from the shaft face seal with self-acting lift pads after 320 hours of steady state endurance testing. The total time of testing on the carbon nosepiece was 338.5 hours. The pretesting lapping marks are still observable. A surface profile trace indicated that the average wear on the surface was less than 5 microinches. A few shallow scratches (50 to 100 microinches) were noticed. The test was concluded after 500 total hours of carbon nosepiece operation. The seal faces had encountered over 50 startups and shutdowns. The leakage rates varied from 11 to 32 SCFM (5.19×10^{-3} to 15.6×10^{-3} SCMS) depending on conditions with leakage generally averaging about 25 SCFM (1.18×10^{-3} SCMS).

SUMMARY OF RESULTS

A design analysis utilizing computer programs was made of seal leakage flow rate and force balance of a shaft face seal with self-acting lift pads using the best available mathematical models. The seal had a 6.5-inch (16.5 cm) nominal diameter dam and 4 design conditions, typical of sump seals in advanced aircraft gas turbines, were considered. (Some of these design conditions exceed the limits of conventional rubbing contact face seal operation.) The investigation included studying the effects of sealing face radial width on opening force and the effect of sealing face angular deformation. The following pertinent results were obtained:

1. The analysis of the shaft face seal with self-acting lift pads shows that this nonrubbing contact face seal design is technically feasible and leakage flow rates less than 1/10 that obtained in conventional labyrinth seal practice are possible.

2. Extensive use was made of molybdenum alloy in the design in order to minimize thermal gradients which cause detrimental seal deformation; in particular the seat, carbon retainer ring, carbon carrier and secondary seal were made from the molybdenum alloy.

3. The seat was structurally isolated from the shaft by a radial spacer in order to mitigate the deformation effects caused by shaft thermal displacement. Further, the seat was clamped through a bellows to provide a predetermined amount of axial clamping and to mitigate clamping distortions.

4. The analysis shows that a characteristic steep gradient of lift force versus gap height of the self-acting geometry is responsible for maintaining the small sealing gap height necessary to limit flow leakage. That is, if the seal tends to open, the lift force drops off rapidly; hence, the closing force increases rapidly. If the seal tends to close, the opposite effect occurs. Thus, the self-acting geometry can provide positive separation and a high gas film stiffness, which is necessary if the nosepiece is to track dynamically the face runout of the seal seat.

5. The analysis also revealed that slight face angular deformation (i.e., 0.001 radians) has a significant effect on the pressure gradient within the sealing faces; thus the seal opening forces are affected.

6. The study shows a narrow radial sealing face width (dam) is desirable because the narrow face has less effect on the opening force when the diverging radial face deformation occurs; further, the calculated leakage of the selected 0.050-inch (0.127 cm) radial dam width is not significantly more than the wider dams studied.

7. For some of the design configurations and operating conditions studied, the flow at the exit of sealing dam was choked. Choked flow occured at pressure ratios as low as 4:1.

Recent tests of this shaft face seal with self-acting lift augmentation design have demonstrated the feasibility of achieving advanced engine operating conditions. The seal appears to be operating as predicted in this design analysis.

APPENDIX A

SYMBOLS

A	pad area, $in.^2$; cm^2
B	constant = $h_m - \frac{\alpha(R_2 - R_1)}{2}$
b	self-acting pad radial width, in.; cm
c	self-acting pad circumferential length, in.; cm
F	sealing dam force, lbf; N
f	feed-groove circumferential length, in.; cm
$\bar{f}$	mean friction factor
H	recess depth plus film thickness, in.; cm
h	film thickness, in.; cm
h_{char}	characteristic film thickness = $\left[\frac{h_1^2 h_2^2}{h_m}\right]^{1/3}$
L	land circumferential length, in.; cm and sealing dam circumferential length, in.; cm
M	Mach number
P	static pressure, psi; N/cm^2
P_1'	static pressure at sealing dam entrance
P_2'	static pressure at sealing dam exit
Q	net leakage (volume) flow rate, SCFM; SCMS
R	recess circumferential length, in.; cm
ΔR	sealing dam width, $R_2 - R_1$, in.; cm
R_c	center of pressure in radial or x-direction, in.; cm

Re	Reynolds number
R	gas constant, universal gas constant/molecular weight, (ft)(lbf)/(lbm)(^{o}R); J/(kg)(K)
r	radius, in.; cm
T	temperature, ^{o}F; K
U	moving seal seat radial surface speed, ft/sec; m/sec
V	moving seal seat circumferential surface speed, ft/sec; m/sec
W	load capacity, lb; kg
X	radial coordinate direction
Y	circumferential coordinate direction
α	relative inclination angle of surfaces, mrad
Δ	recess or pocket depth, in.; cm
Λ_x	compressibility number in radial direction, $6\mu Ub/P_a h_m^2$
Λ_y	compressibility number in circumferential direction, $6\mu Vb/P_a h_m^2$
λ	second viscosity coefficient or coefficient of bulk viscosity
μ	absolute or dynamic viscosity, (lb)(sec)(/in.^{2}; (N)(sec)/cm^2
γ	specific heat ratio, C_p/C_v
Ω	rotational speed, rad/sec
ρ	density, (lbf)(sec^2)/ft^4; kg/m^3

REFERENCES

1. Parks, A. J.; McKibbin, R. H.; and Ng, C. C. W.: Development of Main Shaft Seals for Advanced Air Breathing Propulsion Systems. Rep. PWA-3161, Pratt & Whitney Aircraft (NASA CR-72338), Aug. 14, 1967.

2. Johnson, Robert; Loomis, William R.; and Ludwig, Lawrence P.: Performance and Analysis of Seals For Inerted Lubrication Systems of Turbine Engines. NASA TN D-4761, 1968.

3. Johnson, Robert L.; and Ludwig, Lawrence P.: Shaft Face Seal With Self-Acting Lift Augmentation for Advanced Gas Turbine Engines. NASA TN D-5170, 1969.

4. Ludwig, Lawrence P.; Strom, Thomas N.; Allen, Gordon P.; and Johnson, Robert L.: Improving Performance of Face Contact Seal in Liquid Sodium (400° to 1000° F) by Incorporation of Spiral-Groove Geometry. NASA TN D-3942, 1967.

5. Russell, Terrence E.; Allen, Gordon P.; Ludwig, Lawrence P.; and Johnson, Robert L.: Gas Turbine Face Seal Thermal Deformation and Computer Program for Calculation of Axisymmetric Temperature Field. NASA TN D-5605, 1969.

6. Hawkins, R. M.: Development of Compressor End Seals, Stator Interstage Seals, and Stator Pivot Seals in Advanced Air Breathing Propulsion Systems. Rep. PWA-2875, Pratt & Whitney Aircraft (NASA CR-83786), July 20, 1966.

7. Zuk, John; Ludwig, Lawrence P.; and Johnson, Robert L.: Design Study of Shaft Face Seal With Self-Acting Lift Augmentation. I. Self-Acting Pad Geometry. NASA TN D-5744, 1970.

8. Zuk, John; and Smith, Patricia J.: Computer Program for Viscous, Isothermal Compressible Flow Across a Sealing Dam With Small Tilt Angle. NASA TN D-5373, 1969.

9. Zuk, John; and Smith, Patricia J.: Computer Program for Quasi-One-Dimensional Flow Across a Sealing Dam. Proposed NASA TN.

10. Zuk, John; and Ludwig, L. P.: Investigation of Isothermal Compressible Flow Across a Rotating Sealing Dam, I - Analysis. NASA TN D-5344, 1969.

TABLE I. - DESIGN POINTS

	Design Point			
	1	2	3	4
Velocity, V, ft/sec (m/sec)	200 (61)	500 (153)	450 (137)	500 (152)
Sealed gas pressure, P_1, psia (N/cm^2 abs)	65 (45)	215 (148)	315 (217)	165 (114)
Sealed gas temperature, T_1, ^oF (K)	100 (311)	800 (700)	1300 (977)	800 (700)
Sump pressure, P_2, psia (N/cm^2 abs)	15 (10.3)	15 (10.3)	15 (10.3)	15 (10.3)
Air viscosity, μ, (lb)(sec)/$in.^2$ ((N)(sec)/cm^2)	2.75×10^{-9} (1.9×10^{-10})	4.87×10^{-9} (3.36×10^{-10})	6.00×10^{-9} (4.14×10^{-10})	4.87×10^{-9} (3.36×10^{-10})

TABLE II. - SUMMARY OF SUBSONIC FLOW EQUATIONS FROM REFERENCE 8

Leakage flow rate	$Q = 2.7256 \dfrac{h_{char}^3 L\left(P_1^2 - P_2^2\right)}{\mu RT(R_2 - R_1)}$, SCFM
Pressure distribution	
Parallel film case	$P = P_2\left[1 - \left(1 - \dfrac{P_1^2}{P_2^2}\right)\left(\dfrac{R_2 - r}{R_2 - R_1}\right)\right]^{1/2}$
Small deformation case	$P = P_1\left\{1 + \dfrac{\left[\left(\dfrac{P_2}{P_1}\right)^2 - 1\right] h_2^2 X(2B + \alpha X)}{(R_2 - R_1)h_m(B + \alpha X)^2}\right\}^{1/2}$
Sealing dam force	
Parallel film case	$F = \dfrac{2P_1 L(R_2 - R_1)\left[1 - \left(\dfrac{P_2}{P_1}\right)^3\right]}{3\left[1 - \left(\dfrac{P_2}{P_1}\right)^2\right]}$
Small deformation case	$F = L\int_0^{R_2 - R_1} (P - P_{min})\, dX$, lb (evaluated numerically)
Radial center of pressure	
Parallel film case	$R_c = \dfrac{L(R_2 - R_1)^2}{F}\left\{\dfrac{P_1\left[\dfrac{2}{5}\left(\dfrac{P_2}{P_1}\right)^5 - \dfrac{2}{3}\left(\dfrac{P_2}{P_1}\right)^3 + \dfrac{4}{15}\right]}{\left[1 - \left(\dfrac{P_2}{P_1}\right)^2\right]^2} - \dfrac{P_{min}}{2}\right\}$
Small deformation case	$R_c = \dfrac{L}{F}\int_0^{R_2 - R_1} (P - P_{min})X\, dX$, in. (evaluated numerically

TABLE III

Dam Width		Opening Force Change
in.	cm	lbf
0.100	0.254	6.3
.080	.203	5.1
.050	.127	3.0

TABLE IV. - SUMMARY OF GROSS SHAFT FACE SEAL (WITH SELF-ACTING LIFT AUGMENTATION) CHARACTERISTICS DETERMINED FROM A FORCE BALANCE (PARALLEL FILM)

Design point	Closing force, lbf (kg)		Total force, lbf (kg)	Opening force, lbf (kg)		Operating gap, mils (μm)	Leakage flow rate, SCFM (SCMS)
	Hydrostatic	Spring		Sealing dam	Pad		
1	36.1 (16.4)	6.6 (3.0)	42.7 (19.4)	31.3 (14.2)	11.4 (5.18)	0.25 (6.30)	0.83 (3.92×10^{-4})
2	144.4 (65.6)	6.6 (3.0)	151 (68.7)	141.8 (64.5)	9.2 (4.19)	0.59 (14.9)	17.5 (8.26×10^{-4})
3	216.7 (98.5)	6.6 (3.0)	223.3 (101.5)	214.8 (97.6)	8.5 (3.87)	0.63 (15.9)	25 (1.18×10^{-3})

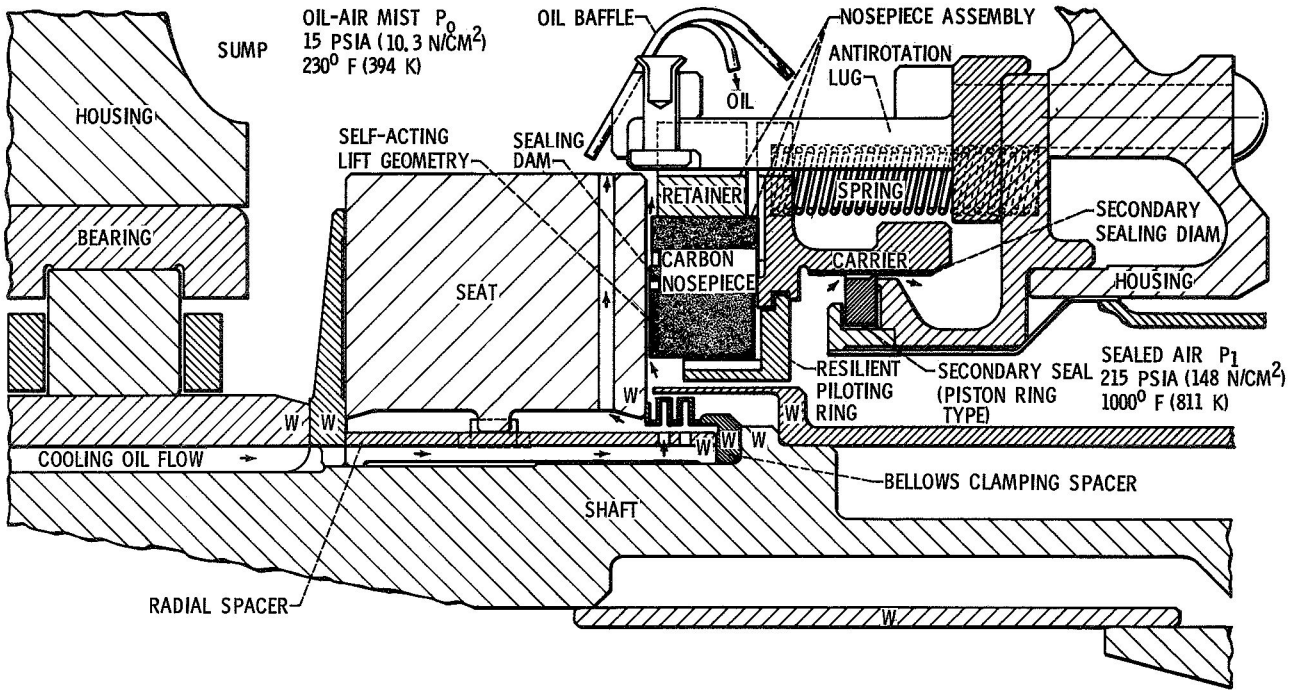

Figure 1. - Shaft face seal with self-acting lift geometry (rotating parts marked W).

COMPRESSIBLE SEALING DAM WITH SMALL TILT ANGLE

SAMPLE PROBLEM

INPUT DATA -

TILT ANGLE = 0.0010 RADIANS

P2,PSIA	P1,PSIA	T,DEG F	VISCOSITY,LB-SEC/FT2	MOLECULAR WEIGHT	CP/CV
15.0000	65.0000	100.	0.39600E-06	28.9660	1.40000

R2,INCHES	R1,INCHES	L,INCHES	RHO,LB-SEC2/FT4	RHO(ROT),LB-SEC2/FT4	NO OF GRID POINTS
3.3150	3.2650	20.6717	0	0	11

N,RPM	V,FT/SEC	CP,BTU/LB-DEG R	SKIP A	SKIP R	SKIP T
1398.00	40.1375	0.24000	F	F	F

BEGIN OUTPUT DATA

GAS CONSTANT,FT-LB/LB(M)-DEG R	RHO(1),LB-SEC2/FT4	A(SOUND SPEED),FT/SEC
53.3522	0.97371E-02	1160.08

L,INCHES	AREA,IN2	SPEED,RPM	V,FT/SEC
20.6717	1.03358	1398.00	40.1375

MEAN FILM INCHES	M(OUT) LB/MIN	Q SCFM	MACH (MAX)	RE(P)	RE(R)	KNUDSEN NUMBER	F LB	STIFF LB/IN	XC INCHES	XC BAR	F BAR
0.100E-02							ANALYSIS NOT VALID				
0.900E-03							ANALYSIS NOT VALID				
0.800E-03							ANALYSIS NOT VALID				
0.700E-03							ANALYSIS NOT VALID				
0.600E-03							ANALYSIS NOT VALID				
0.500E-03							ANALYSIS NOT VALID				
0.450E-03							ANALYSIS NOT VALID				
0.400E-03							ANALYSIS NOT VALID				
0.350E-03	0.177	2.316	0.754	288.097	19.865	0.008	29.507	-0.464E 04	0.181E-01	0.363	0.571
0.300E-03	0.111	1.451	0.558	182.424	16.879	0.009	29.220	-0.677E 04	0.180E-01	0.361	0.565
0.250E-03	0.636E-01	0.832	0.391	106.207	13.893	0.011	28.819	-0.954E 04	0.179E-01	0.359	0.558
0.200E-03	0.320E-01	0.419	0.253	54.671	10.907	0.014	28.221	-0.147E 05	0.177E-01	0.355	0.546
0.150E-03	0.130E-01	0.170	0.144	23.044	7.924	0.019	27.240	-0.262E 05	0.174E-01	0.349	0.527
0.100E-03	0.346E-02	0.452E-01	0.064	6.559	4.960	0.029	25.387	-0.506E 05	0.169E-01	0.338	0.491

MEAN FILM,INCHES	POWER,H.P.	SHEAR HEAT,BTU/MIN	DEL(T),DEG F	TORQUE,FT-LB
0.100E-02				ANALYSIS NOT VALID
0.900E-03				ANALYSIS NOT VALID
0.800E-03				ANALYSIS NOT VALID
0.700E-03				ANALYSIS NOT VALID
0.600E-03				ANALYSIS NOT VALID
0.500E-03				ANALYSIS NOT VALID
0.450E-03				ANALYSIS NOT VALID
0.400E-03				ANALYSIS NOT VALID
0.350E-03	0.28545E-03	0.12109E-01	0.28497	0.67381E-02
0.300E-03	0.33302E-03	0.14127E-01	0.53089	0.78611E-02
0.250E-03	0.39963E-03	0.16952E-01	1.11107	0.94333E-02
0.200E-03	0.49954E-03	0.21190E-01	2.75934	0.11792E-01
0.150E-03	0.66605E-03	0.28254E-01	9.05200	0.15722E-01
0.100E-03	0.99907E-03	0.42381E-01	51.1084	0.23583E-01

Figure 2. - An example of a computer printout sheet. Illustrates data for design point one and a 1 milliradian diverging seal surface separation.

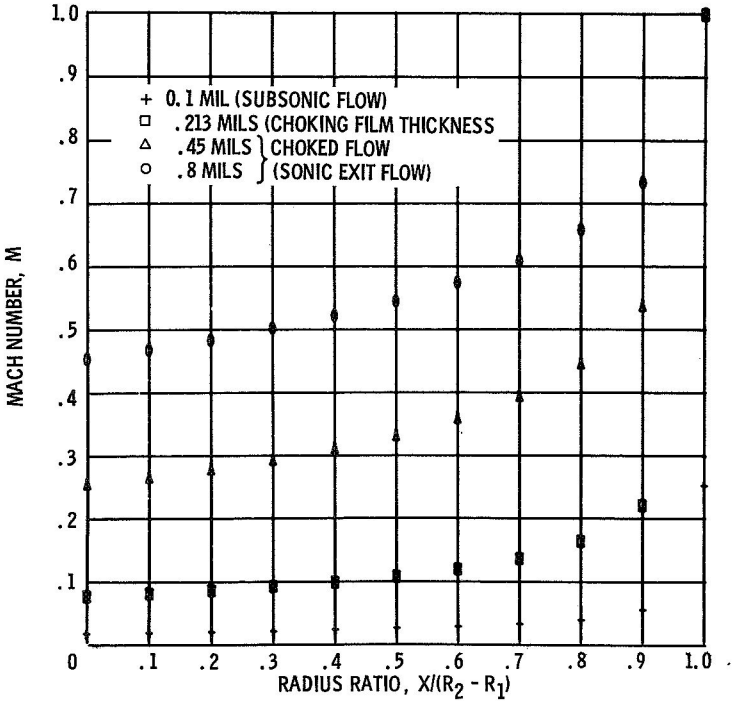

Figure 3. - An example of a computer output. microfilm plot. Mach number variation is shown as a function of radial distance along the sealing dam for several film thicknesses.

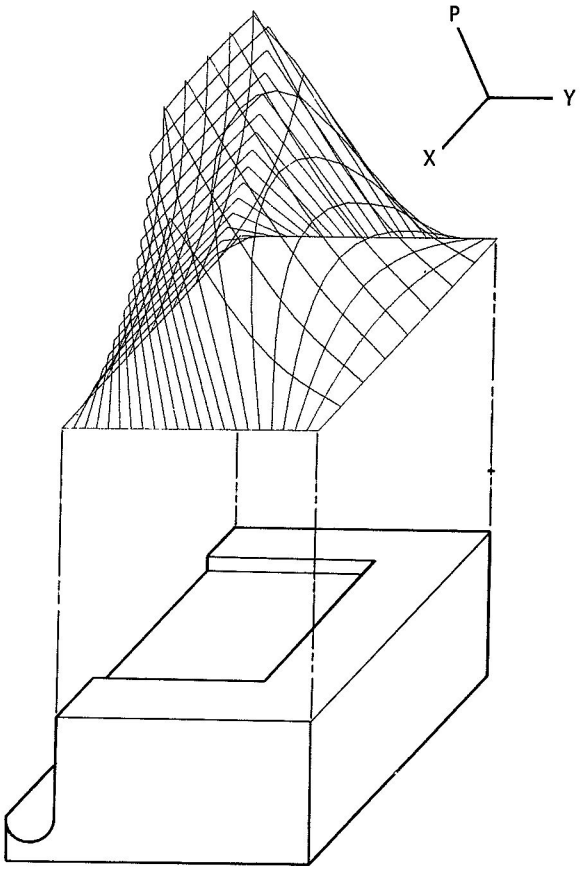

Figure 4. - An example of a Calcomp computer plot of pressure distribution across a shrouded Rayleigh lift pad.

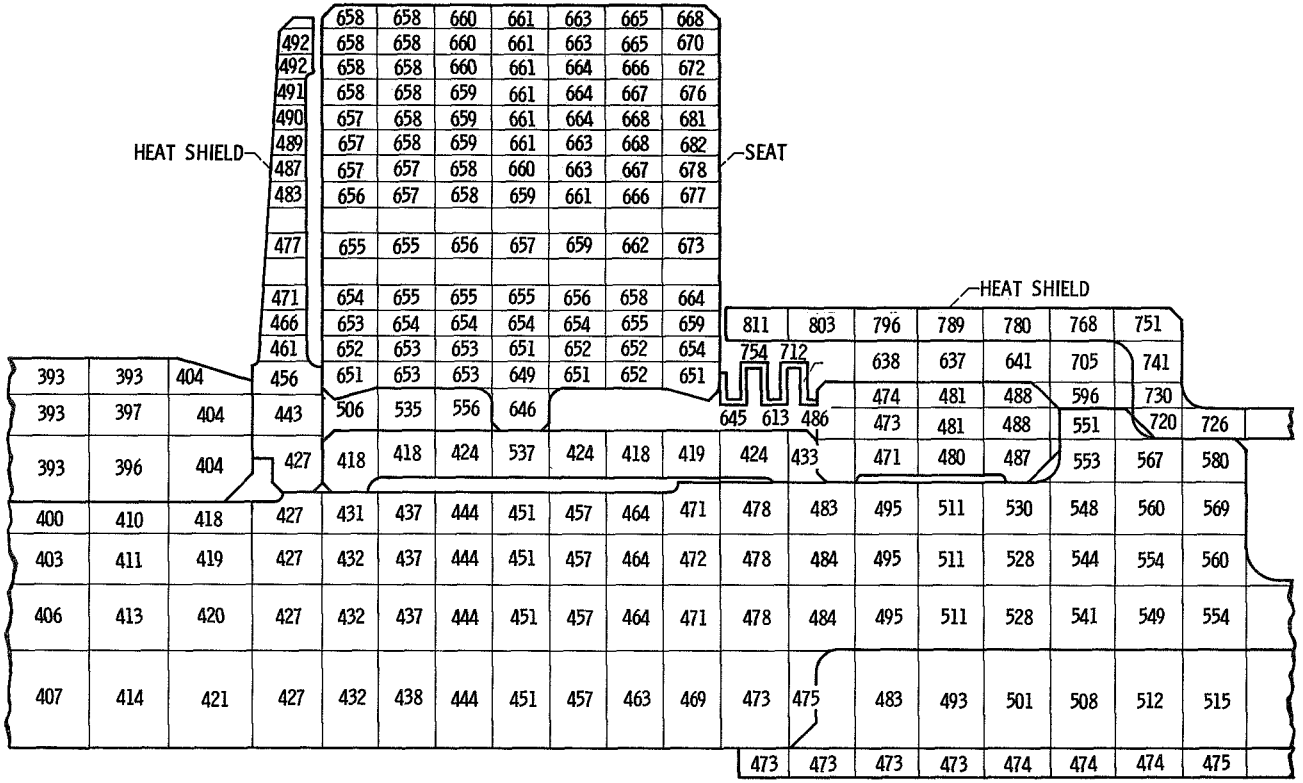

Figure 5. - Calculated temperature field of seat assembly; design conditions: 165 psia (114 N/cm^2) sealed pressure, 500 ft/sec (153 m/sec) mean sliding speed, 800^0 F (700 K) sealed gas temperature. (Temperatures are expressed in ^{0}F.)

E-5917

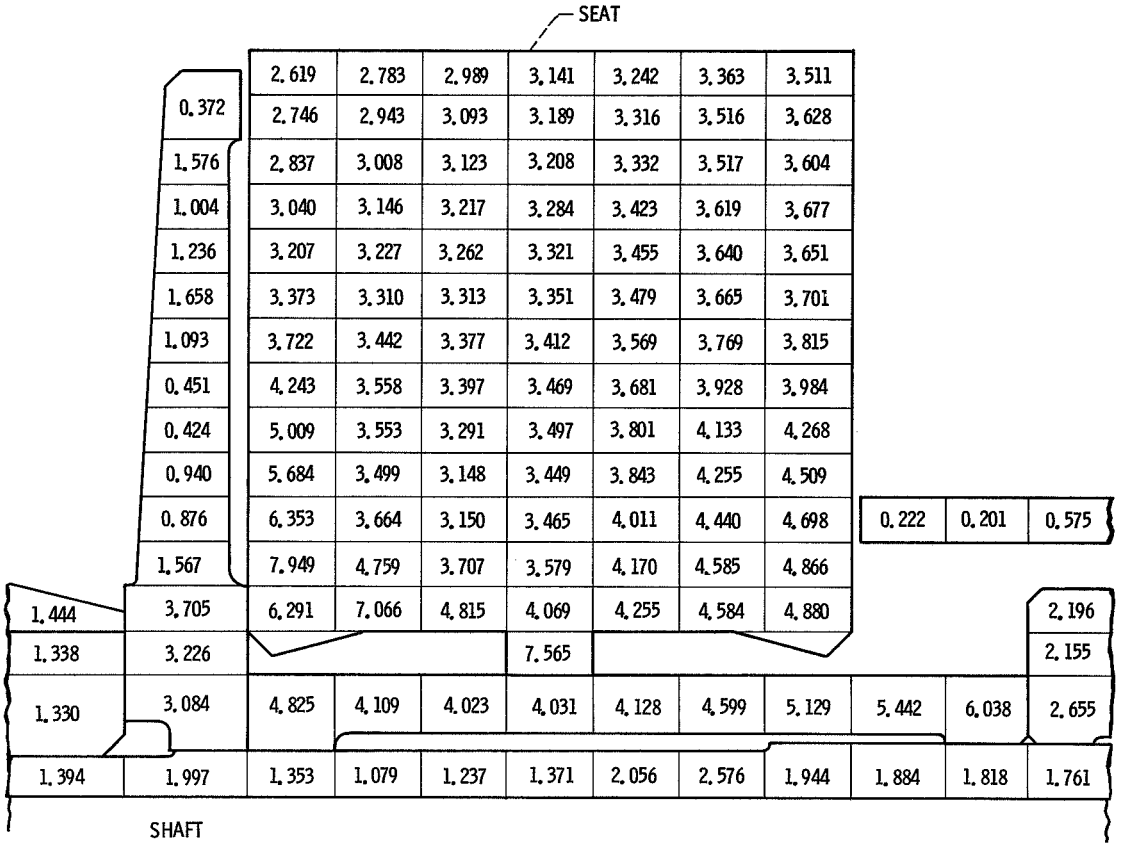

	0.372	2.619	2.783	2.989	3.141	3.242	3.363	3.511			
		2.746	2.943	3.093	3.189	3.316	3.516	3.628			
	1.576	2.837	3.008	3.123	3.208	3.332	3.517	3.604			
	1.004	3.040	3.146	3.217	3.284	3.423	3.619	3.677			
	1.236	3.207	3.227	3.262	3.321	3.455	3.640	3.651			
	1.658	3.373	3.310	3.313	3.351	3.479	3.665	3.701			
	1.093	3.722	3.442	3.377	3.412	3.569	3.769	3.815			
	0.451	4.243	3.558	3.397	3.469	3.681	3.928	3.984			
	0.424	5.009	3.553	3.291	3.497	3.801	4.133	4.268			
	0.940	5.684	3.499	3.148	3.449	3.843	4.255	4.509			
	0.876	6.353	3.664	3.150	3.465	4.011	4.440	4.698	0.222	0.201	0.575
	1.567	7.949	4.759	3.707	3.579	4.170	4.585	4.866			
1.444	3.705	6.291	7.066	4.815	4.069	4.255	4.584	4.880			2.196
1.338	3.226				7.565						2.155
1.330	3.084	4.825	4.109	4.023	4.031	4.128	4.599	5.129	5.442	6.038	2.655
1.394	1.997	1.353	1.079	1.237	1.371	2.056	2.576	1.944	1.884	1.818	1.761

Figure 6. - Calculated stresses in seat assembly due to combined centrifugal and thermal effects; design conditions: 165 psia (114 N/cm^2) sealed pressure, 500 ft/sec (153 m/sec) mean sliding velocity, 800^0 F (700 K) sealed gas temperature. (Stresses are expressed in psix10^{-4}.)

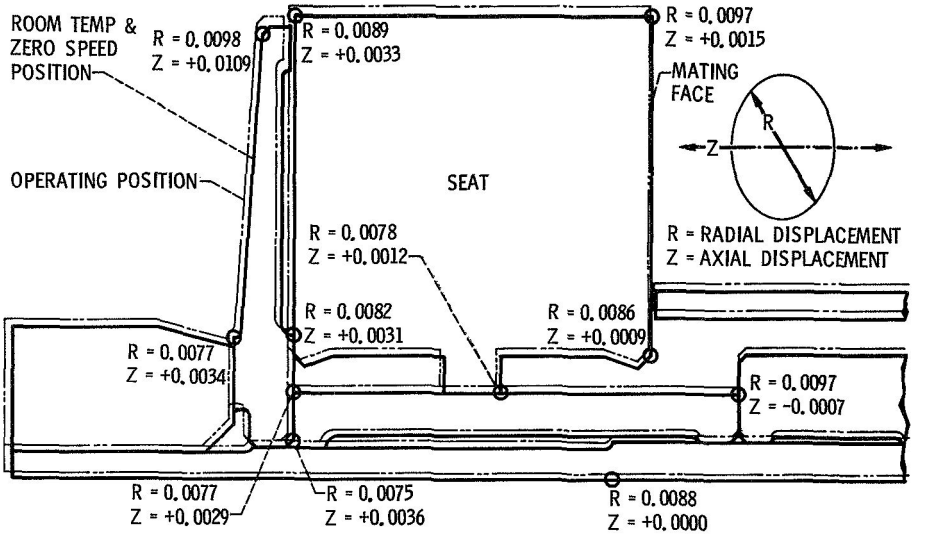

Figure 7. - Displacement of seat assembly due to centrifugal and thermal effects; Design conditions: 165 psia (114 N/cm^2 abs) sealed pressure, 500 ft/sec (153 m/sec) mean sliding speed, 800° F (700 K) sealed gas temperature. (Displacements are expressed in inches.

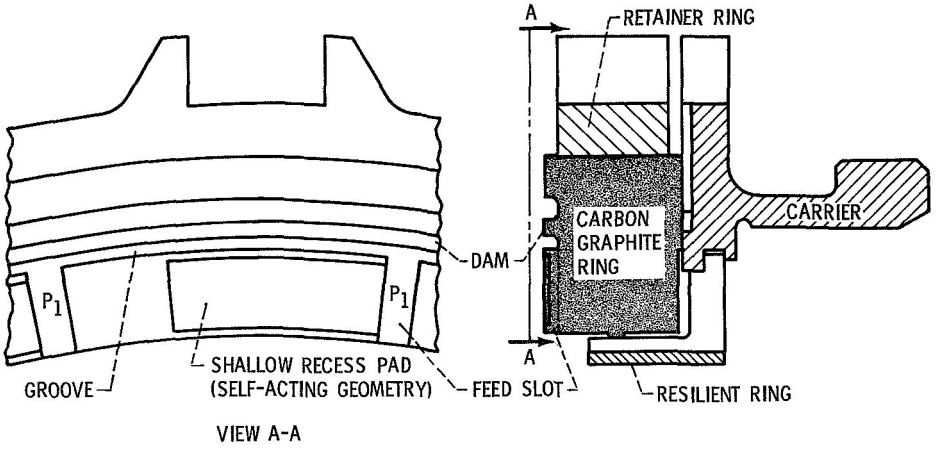

Figure 8. - Face seal with self-acting pads.

E-5917

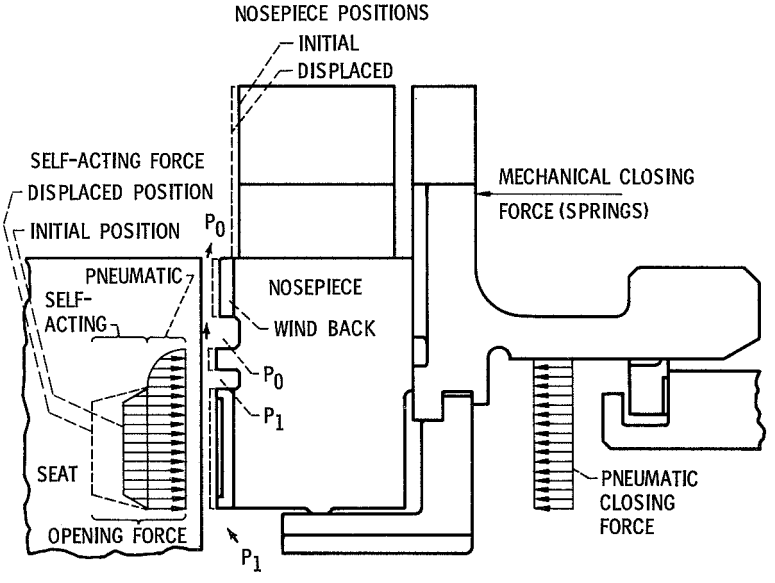

Figure 9. - Mechanical, pneumatic, and self-acting forces acting on seal nosepiece.

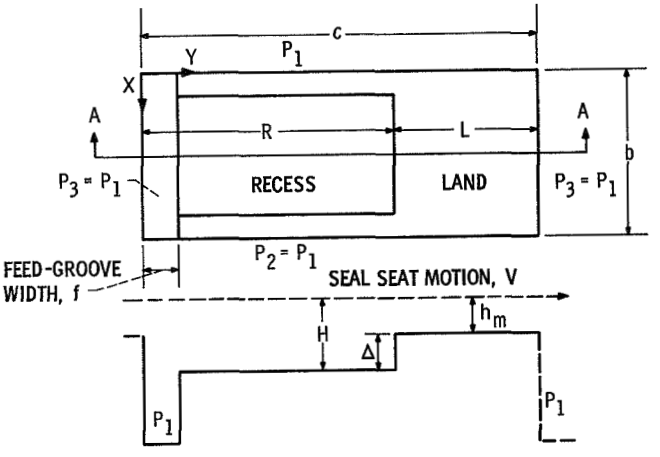

SECTION A-A

(a) Lift pad mathematical model.

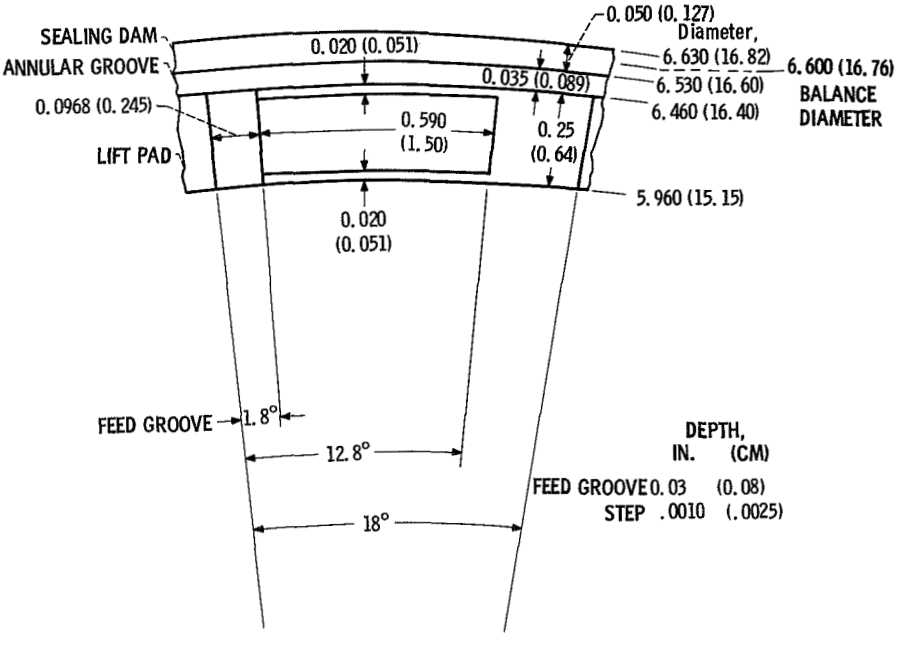

(b) Final design details of sealing dam and of self-acting pad geometry. Dimensions are in inches (cm).

Figure 10. - Self-acting geometry.

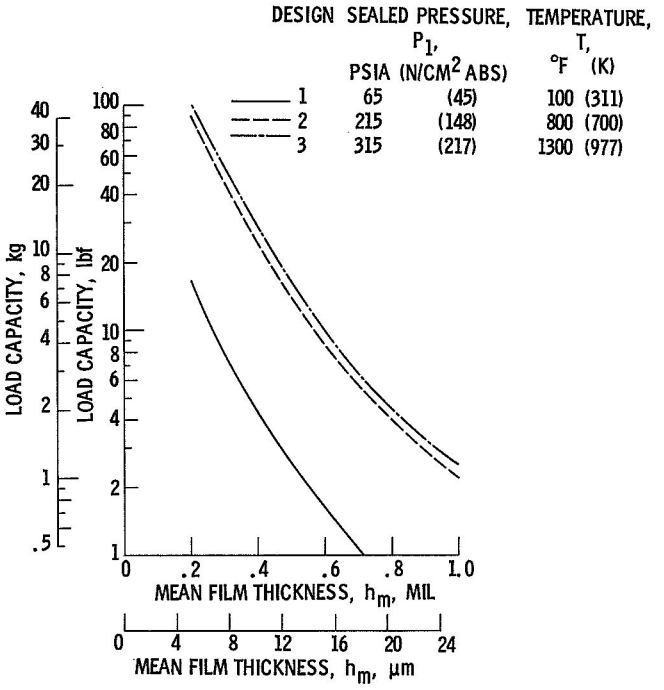

Figure 11. - Load capacity of shrouded self-acting pads as function of film thickness. Number of pads, 20; recess length to-land length ratio, 1.4. From ref. 7.

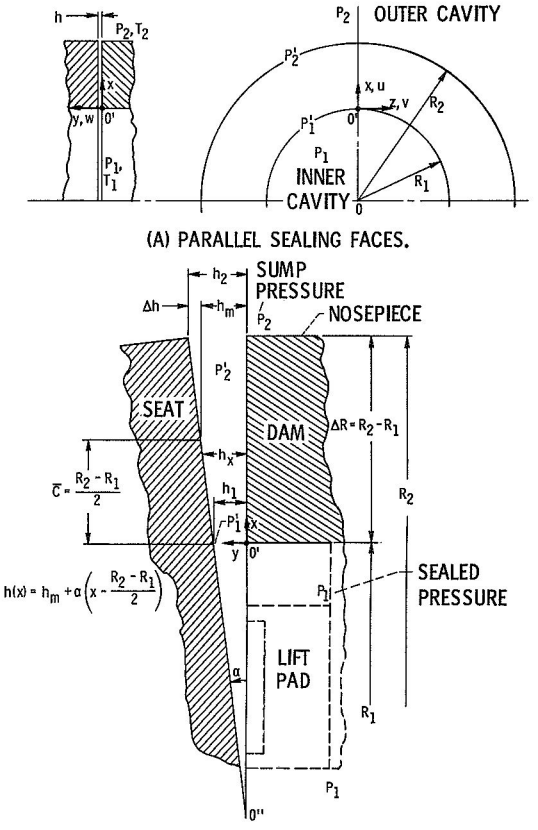

(A) PARALLEL SEALING FACES.

(B) SEALING FACES WITH SMALL TILT (FACE DEFORMATION).

Figure 12. - Model and notation of sealing faces (dam).

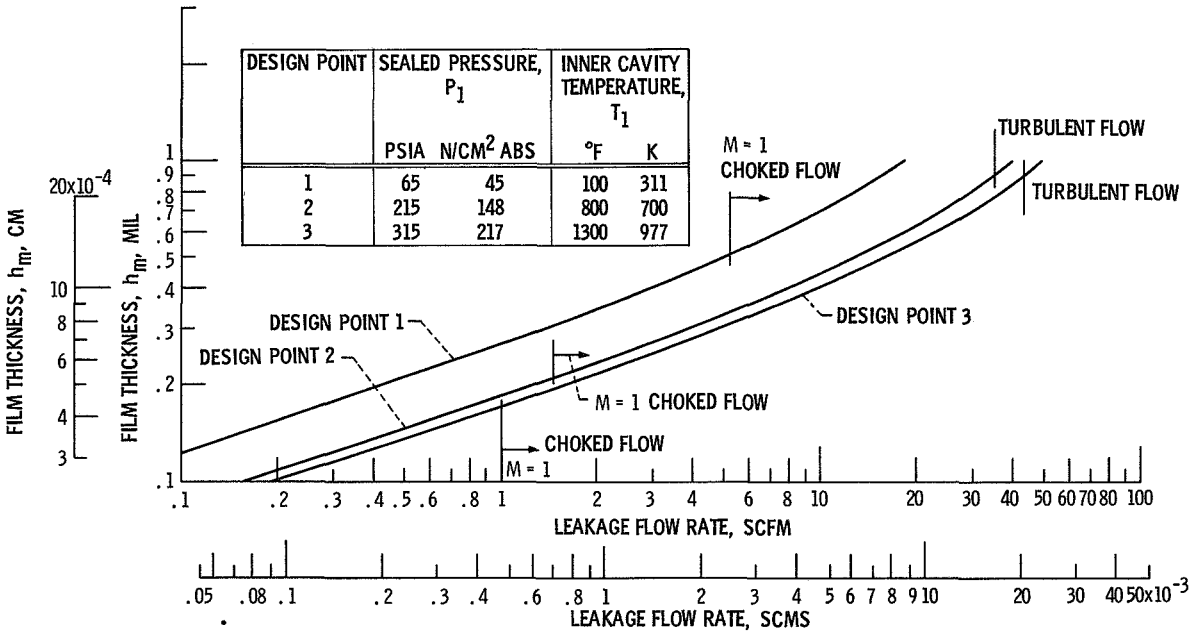

Figure 13. - Effect of operating point (pressure and temperature) on seal gas leakage parallel sealing surfaces ($\alpha = 0$; sealing face radial length, 50 mils (0.127 cm); sump pressure, $P_2 = 15$ psia (10.3 N/cm^2 abs); sealed fluid, air.

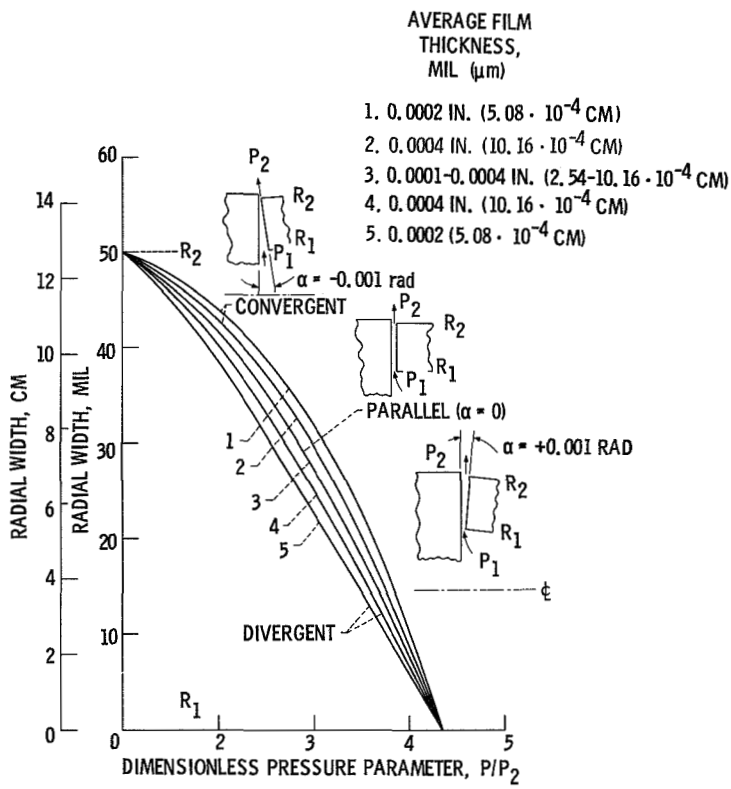

Figure 14. - Pressure ratio as a function of average film thickness for design point 1; sealed pressure, 65 psia (45 N/cm^2 abs); sealed gas temperature, 100° F (311 K); sump pressure 15 psia (10.3 N/cm^2 abs); radial dam width, 0.050 in. (0.127 cm).

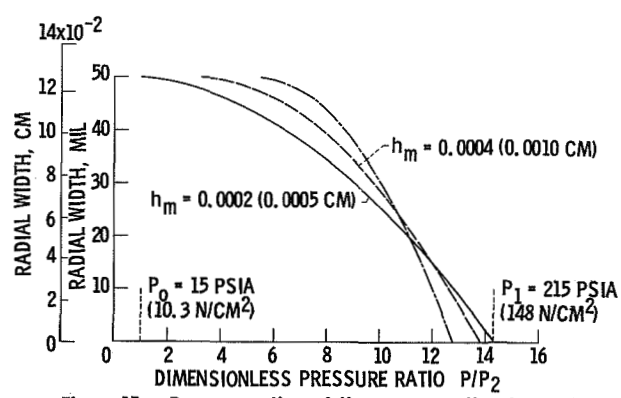

Figure 15. - Pressure ratio variation across sealing dam radial width for several parallel film thicknesses represening subsonic and choked flow conditions. Seal velocity 500 ft/sec (148 m/sec), sealed pressure 215 psia (148 N/cm^2), gas temperature 800° F (700 K).

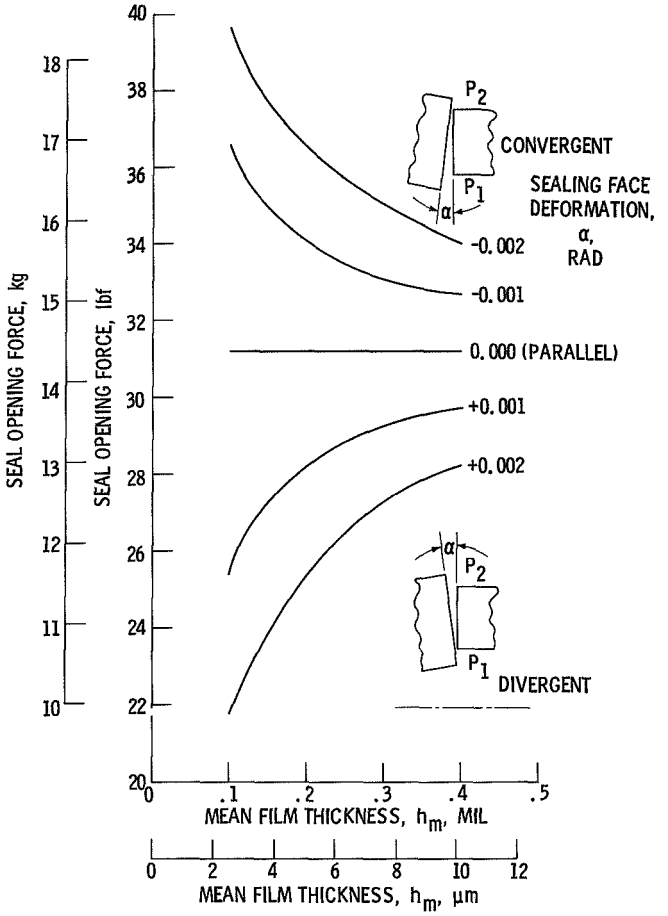

Figure 16. - Effect of sealing face deformation on opening force. Design point 1: sealed pressure, P_1, 65 psia (45 N/cm^2 abs); sealed gas temperature, T_1, 100° F (311 K); sump pressure, P_2, 15 psia (10.3 N/cm^2 abs); radial dam width, 50 mils (0.127 cm).

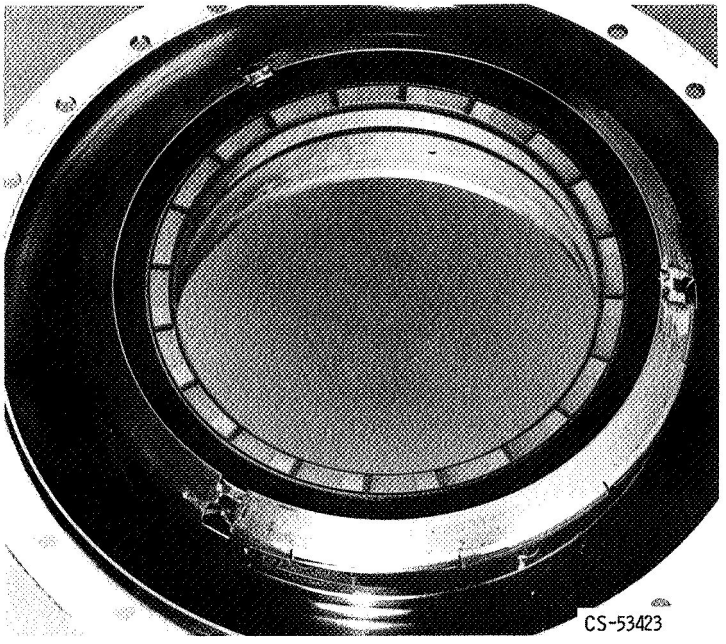

Figure 17. - Gas-film seal assembly nosepiece after 120-hour endurance test.

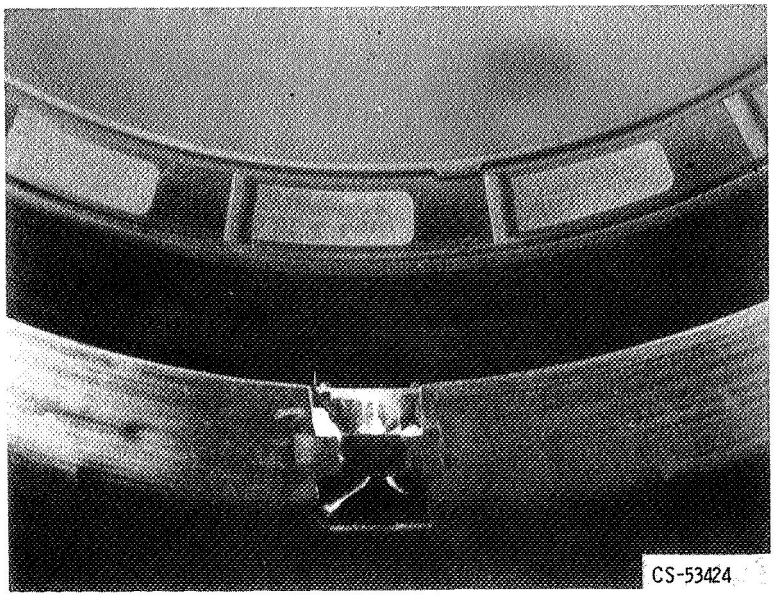

Figure 18. - Close-up of carbon nosepiece of the gas-film seal after 200 hours of endurance testing. Total time on seal: 338.5 hours.